Mechanokinetics of Rapid Tension Recovery in Muscle: The Myosin Working Stroke Is Followed by a Slower Release of Phosphate

David A. Smith* and John Sleep†
*Department of Physiology, Monash University, Clayton, Victoria 3800, Australia; and †Randall Centre, King's College London, London SE1 1UL, United Kingdom

ABSTRACT Crystallographic and biochemical evidence suggests that the myosin working stroke that generates force in muscle is accompanied by the release of inorganic phosphate (Pi), but the order and relative speed of these transitions is not firmly established. To address this problem, the theory of A. F. Huxley and R. M. Simmons for the length-step response is averaged over elastic strains imposed by filament structure and extended to include a Pi-release transition. Models of this kind are applied to existing tension-recovery data from length steps at different phosphate concentrations, and from phosphate jumps upon release of caged phosphate. This body of data is simulated by the model in which the force-generating event is followed by Pi release. A version in which the Pi-release transition is slow provides a better fit than a version with rapid Pi release and a slow transition preceding force generation. If Pi is released before force generation, the predicted rate of slow recovery increases with the size of the step, which is not observed. Some implications for theories of muscle contraction are discussed.

INTRODUCTION

Some time ago, Huxley and Simmons (1971) observed asymmetric rapid recovery of tension after quick release or quick stretch of a frog muscle, and interpreted their findings in terms of a unitary force-generating transition in myosin after binding to actin. Their observations still constitute clear evidence for what is now the ''swinging lever-arm'' model of muscle contraction (Cooke, 1997; Geeves and Holmes, 1999; Holmes, 1997), in which the neck region of each myosin ''head'' (myosin-S1) generates force by making a working stroke; this model is supported by atomic structure determinations (Dominguez et al., 1998; Fisher et al., 1995; Rayment et al., 1993) and a great variety of experiments in the last decade. However, the two-state model of Huxley and Simmons for length-step recovery needs to be updated in the face of evidence that the force-generating transition is kinetically coupled to the release of phosphate; after a quick stretch, rapid tension recovery shows two exponential phases, 2 a and 2 b (Davis and Rodgers, 1995; Ranatunga et al., 2002), and the rate of the slower phase (2 b) increases strongly with the concentration of free phosphate in the fiber (from 10 to 100s^{-1} for 1–25 mM Pi). In addition, the original two-state model requires unduly small values of myosin stiffness to avoid incorrect predictions for the amplitude of recovery.

In this article, we develop generalizations of the Huxley-Simmons model to clarify the relationship between the force-generating and Pi-release events in the muscle cross-bridge cycle. These models also involve transitions between a limited number of bound states, which on the timescale of rapid recovery are kinetically isolated from the rest of the cycle. To account for the slower phase, a correspondingly slow transition must be included in this kinetic scheme. Does the slow transition come before or after the force generating transition? Is phosphate release directly associated with the slow transition? These questions can be answered from a comparative study of the predictions of kinetic models for step perturbations, notably length steps and phosphate jumps. In caged-Pi experiments (Millar and Homsher, 1990; Dantzig et al., 1992), the rate of tension fall produced by a phosphate jump increases hyperbolically with jump size (from 20 to 80 s^{-1} for 1–12 mM of final Pi), suggesting that the binding of Pi is coupled to a reversal of the working stroke. Phosphate jumps in either direction can be produced in solution-exchange experiments on myofibrils (Tesi et al., 2000). In this article, three bound-state models are defined and tested against the above data. Finally, we need to show how the optimum model can be embedded in the actin-myosin-ATP cycle.

To predict rapid recovery transients, consider a model of the kind for the bound head, where 1, 2 are prestroke states, $2 \rightarrow 3$ is the force-generating transition, and 3, 4 are poststroke states. The rate constants of the force-generating transition generally depend on elastic strain x in the prestroke states, which is imposed when myosin binds to form a cross-bridge. Biochemically, 1 is the A.M.ADP.Pi state formed by the binding of M.ADP.Pi to actin and 4 is the dominant A.M.ADP state. For biphasic responses, either the first or the last transition is assumed to be slower than force generation. The remaining transition is assumed to be very fast, permitting a reduction to three states. Thus

Submitted December 2, 2003, and accepted for publication March 29, 2004.
Address reprint requests to Dr. David Smith, Dept. of Physiology, Monash University, Clayton, Victoria 3800, Australia. Tel.: 61-3-9905-2518; Fax: 61-3-9905-2547; E-mail: david.smith@med.monash.edu.au.

0006-3495/04/07/442/15 $2.00
doi: 10.1529/biophysj.103.037788

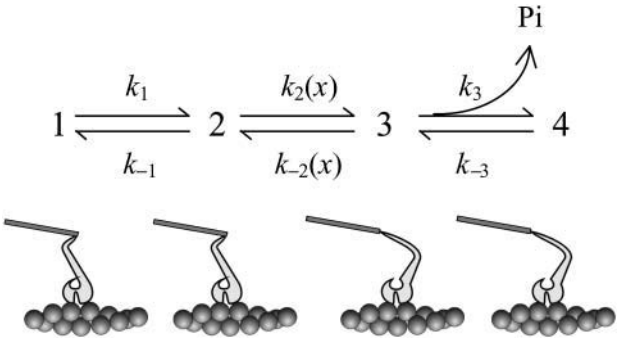

SCHEME 1

Version *A*: 1→2 is very fast (state 1 can be omitted); Pi is released slowly in 3→4.

Version *B*: 1→2 is slow; Pi is released very rapidly in 3→4.

We have also investigated a model in which Pi is released before force generation. In this case, the slow transition must be identified with release of Pi, to comply with the slow net rate of Pi release ($75 s^{-1}$) observed in solution-mixing experiments (White et al., 1997).

Tension response in the muscle fiber is generated by the combined response of all myosin heads in the half sarcomere. The vernier spacing of heads on the thick filament and binding sites on the thin filament guarantees a spatial distribution of elastic strains, imposed by the longitudinal mismatch between heads and sites. This distribution is not present in the model of Huxley and Simmons, and Huxley and Tideswell (1996) have shown that strain-averaging can generate the observed amplitude of recovery without requiring elastically weak cross-bridges. All models studied in this article include strain-averaging as above. With current estimates of 1–2 pN/nm for myosin stiffness (Dobbie et al., 1998, Linari et al., 1998), the probabilities of prestroke and postforce states vary rapidly with strain, and the theory is simplified by assuming that all bound heads with strains above some critical value are in prestroke states, whereas the remainder are in poststroke states.

Strain-averaging implies that the predicted tension responses are a continuous superposition of exponentials

$$\Delta T(t) = \int_0^\infty A(r)\exp(-rt)dr,$$

where the distribution $A(r)$ is determined by the initial state. Thus upward and downward phosphate jumps of the same magnitude, ending at the same final phosphate concentration, could give different apparent rates of tension change (Tesi et al., 2000). Computational procedures exist for fitting measured transients in this way (K. Burton, R. M. Simmons, and J. Sleep, unpublished).

Model calculations were made by assuming that the thick and thin filaments are rigid structures, so that individual heads act independently. However, the filaments are known to be elastically compliant (Huxley et al., 1994, Wakabayashi et al., 1994). To a first approximation, compliance in the filaments can be absorbed into an apparent elastic constant for each head; limitations of this approach are considered in the Discussion section.

Strain-dependent kinetic models are developed in the next section. The method of calculation is introduced with a two-state model that predicts the faster phase of rapid length-step recovery; this model is tested against published data for shortening steps. Various three-state models are then defined and their kinetics explained in terms of eigenvalues of the reaction matrix. In the following sections, these models are applied to length-step and phosphate-jump perturbations. Finally, we consider the implications of our results for models of muscle contraction, and their relation to current views on myosin structure and molecular mechanisms for force generation and release of phosphate.

KINETIC MODELS FOR RAPID RECOVERY

A two-state model

The myosin working stroke is the force-generating transition thought to be responsible for the faster component of rapid recovery. Let 2 and 3 be prestroke and poststroke states of the bound myosin, with tensions kx and $k(x + h)$, where k is myosin stiffness and x the head-site mismatch. The transitions are generally strain-dependent:

$$2 \underset{k_{-2}(x)}{\overset{k_2(x)}{\rightleftharpoons}} 3$$

SCHEME 2

The difference in their strain energies is the quantity $\frac{1}{2}k(x+h)^2 - \frac{1}{2}kx^2 = kh(x + h/2)$, which appears in the equilibrium constant $K_2(x) \equiv k_2(x)/k_{-2}(x)$. The observed rate of recovery increases rapidly with the size of a release (Ford et al., 1977), which suggests that this strain energy appears entirely in the forward rate; $k_2(x) = k_2 \exp(-kh(x + h/2)/k_BT)$ (k_B, Boltzmann's constant; T, absolute temperature) while $k_{-2}(x) = k_{-2}$. However, if the working stroke is a thermally activated transition between the stable orientations of states 2 and 3, the Gibbs-energy landscape should be as in Fig. 1, where these states are defined by narrow energy wells with respect to angle θ of the lever arm. In this case, $kh(x + h/2)$ is a strain-energy barrier to the forward transition when positive, and the above formulae apply only for $x > -h/2$. For $x < -h/2$, the strain barrier $-kh(x + h/2)$ inhibits the reverse transition, so $k_{-2}(x) = k_{-2}\exp(kh(x + h/2)/k_BT)$, $k_2(x) = k_2$. Rate curves predicted by both forms are presented.

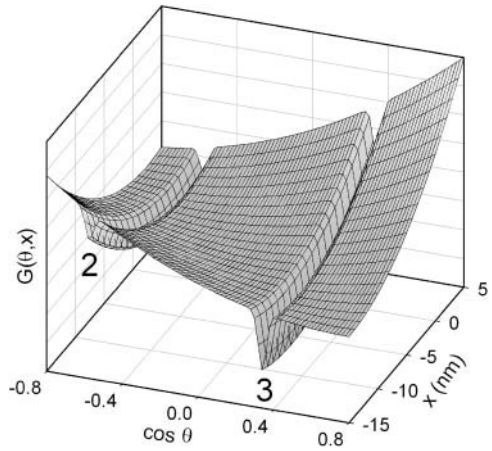

FIGURE 1 Hypothetical Gibbs-energy landscape seen by a bound myosin head as a function of angle θ between lever arm and filament, and elastic strain x in the prestroke state (Eisenberg et al., 1980; Wood and Mann, 1981). The prestroke state (*2*) and poststroke state (*3*) are defined by sharp angular potential wells. At intermediate angles, the lever arm is assumed free to rotate unless tethered to the thick filament, when rotation occurs against the elastic strain energy $\frac{1}{2}k(x + R(\cos\theta - \cos\theta_2))^2$ for a lever-arm of length R. The working stroke to state 3 is $h = R(\cos\theta_3 - \cos\theta_2)$, here set at 10 nm. Note that strain creates an additional energy barrier to the force-generating transition $2 \rightarrow 3$ for $x > -h/2 = -5$ nm, whereas more negative strains ($x < -5$ nm) create an additional barrier to the reverse transition. The resulting kinetics is described in the main text.

Muscle tension $T(t)$ per head at time t is calculated from the formula

$$T(t) = \frac{k}{b}\int_{-b/2}^{b/2}\{xp_2(x,t) + (x+h)p_3(x,t)\}dx \qquad (1)$$

in terms of state probabilities for a head with strain x, averaged over the actin half-repeat distance $b = 36.5$ nm. The joint probability $P(x) = p_2(x,t) + p_3(x,t)$ of both bound states is conserved on the timescale of rapid recovery. The change of population in state 3, measured from final equilibrium, is $\Delta p_3(x,t) = \Delta p_3(x)\exp(-r_2(x)t)$, where $r_2(x) = k_2(x) + k_{-2}(x)$. The initial deviation is generated by the length step Δl on an existing equilibrium:

$$\Delta p_3(x) = \left\{\frac{K_2(x-\Delta l)}{1+K_2(x-\Delta l)} - \frac{K_2(x)}{1+K_2(x)}\right\}P(x-\Delta l). \quad (2)$$

Here x is prestroke strain after the step.

We now assume that $K_2(x)$varies so rapidly with x that, in internal equilibrium, almost all heads are either in state 2 ($K_2(x) \ll 1$) or state 3 ($K_2(x) \gg 1$). Let x_* be the critical strain for which $K_2(x_*) = 1$, giving

$$x_* = -h/2 + \ln K_2/\gamma \quad (\gamma \equiv kh/k_BT). \qquad (3)$$

Heads with $x > x_*$ are in the prestroke state and those with $x < x_*$ in the poststroke state. Thus the bracketed expression in Eq. 2 can be replaced by a box function equal to unity for $x_* < x < x_* + \Delta l$ and zero outside this range. This ''box approximation'' is valid if $\gamma\Delta l \gg 1$. For example, $\gamma = 2$ nm^{-1} if $k = 1$ pN/nm and $h = 8$ nm, so length steps should be in excess of 0.5 nm. Then the tension transient relative to final tension T_2 is

$$\Delta T(t) \approx \frac{kh}{b}\int_{x_*}^{x_*+\Delta l} P(x-\Delta l)\exp\{-r_2(x)t\}\,dx \qquad (4)$$

and arises only from heads with strains in the range $(x_*, x_* + \Delta l)$. The response is an average of exponentials with very different rate constants, particularly for large releases.

Tension transients from length steps have been calculated from this formula, assuming that $P(x)$ is constant. Time courses as a fraction of the total tension change $T_1 - T_2$, and overall rates of recovery as a fraction of k_{-2}, are shown in Fig. 2 as functions of $\gamma\Delta l$. The recovery rate decreases strongly with step size; fitting this curve to experimental data for length releases, where phase 2 *a* is the dominant response, is an important test of the model. With all strain dependence in the forward rate, the predicted recovery rate $R(\Delta l)$ for releases is empirically fitted by the formula $R(\Delta l)/k_{-2} \approx 1 + \exp(-\eta\gamma\Delta l)$,with $\eta = 0.37$, which is not as steep as the function $1 + \exp(-\gamma\Delta l)$predicted without sarcomere averaging. Published rate data for the frog are fitted for small releases if $\gamma = 1.2$ nm^{-1} ($kh = 4.8$ pN). For releases of more than 4.5 nm, the data fall below the predicted curve and a better fit is obtained by using the rate constants derived from Fig. 1. However, recovery from large releases is very fast and observed rate constants may be limited by instrumental factors.

The joint bound-state probability $P(x)$ is determined by the whole cross-bridge cycle and lies beyond the scope of restricted bound-state models. For small steps, it is reasonable to assume that $P(x)$ is constant within the range of strains involved. For larger steps, the amount recovery is controlled by the domain of support of $P(x)$ (~10 nm), and Eq. 4 gives the formula

$$T_1(\Delta l) - T_2(\Delta l) \approx \frac{kh}{b}\int_{x_*-\Delta l}^{x_*} P(x)dx, \qquad (5)$$

valid in the box approximation. This result is useful in understanding the characteristic shape of the T_2 curve. Thus for large steps in either direction, $|T_1 - T_2|$ should be independent of step size and equal to *khp*, where p is the fraction of heads in states 2 and 3; each bound head contributes the unitary force *kh* from the working stroke after release, or –*kh* from its reversal after stretch. It is tempting to use Eq. 5 to obtain the form of $P(x)$ from experimental T_1 and T_2 curves. In practice, this approach runs into difficulties because measured values of T_1 and T_2 are usually normalized to isometric tension T_0, whose value per myosin head reflects

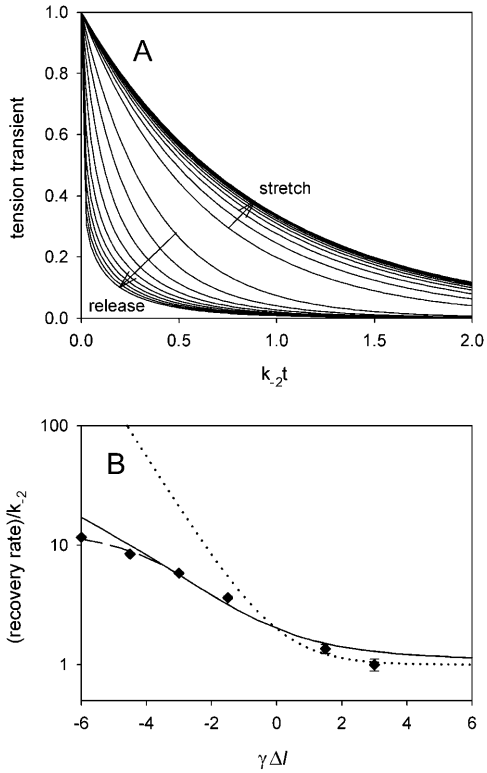

FIGURE 2 (*A*) Phase-2 tension transients, normalized to unity, calculated from the two-state model with strain averaging for various length steps. With $P(x)$ constant and all strain-dependent kinetics in the forward rate $k_2(x)$, Eq. 4 predicts universal curves $\Delta T(t)/\Delta T(0) = e^{-\tilde{t}}(E_1(\tilde{t}e^{-\Delta\tilde{l}}) - E_1(\tilde{t}))/\Delta\tilde{l}$ as functions of scaled time $\tilde{t} \equiv k_{-2}t$ and scaled length steps $\Delta\tilde{l} \equiv \gamma\Delta l = -10, -9, \ldots, -1, 1, \ldots, 9, 10$, where $\gamma \equiv kh/k_BT$. $E_1(x)$ is the exponential integral of order 1 (Press et al., 1992). (*B*) Step dependence of the rate of recovery, to 1/e of the total change, from the above curves (*solid line*). The function $1 + \exp(-\gamma\Delta l)$ (*dotted line*) is predicted in the absence of sarcomere averaging (Huxley and Simmons, 1971). The solid curve approximates data of Ford et al. (1977), (♦) for the frog at 4°C, scaled with $k_{-2} = 345\ s^{-1}$ and $\gamma = 1.2\ nm^{-1}$ ($kh = 4.8$ pN), except for large releases where recovery is very fast. Rate constants determined experimentally as inverse half-times have been multiplied by 0.693. The dashed curve shows the effect of using the bounded form of $k_2(x)$ (see main text) with $K_2 = 20$; this curve falls below the solid curve for $\gamma\Delta l < -\ln K_2 = -3.0$.

uncertainties in the concentration of myosin heads (He et al., 1997). The T_1 curve is also determined by the fraction of bound heads: this fraction may reflect bound states other than those linked by the force-generating transition. For these reasons, the focus in this article is on predicting rates rather than amplitudes of phase 2 recovery.

Models with Pi release after force generation

A model of this kind with four states was described in the introduction. There are two ways of reducing it to just three bound states and hence two phases of rapid recovery. In version *A*, the Pi-release step is slower than the force-generating transition and accounts for the slower phase of the recovery. In version *B*, the slower phase arises from a transition between two prestroke states, and Pi is released very rapidly, namely faster than force generation. To avoid a proliferation of subscripts, states with the same numeric label have the same biochemical identity in both versions, and the same notations are used for rates of transition.

There is a common formula for calculating the tension response to a step perturbation:

$$\Delta T(t) = \frac{kh}{b}\sum_{\pm}\int C_{\pm}(x)\exp(-\lambda_{\pm}(x)t)dx, \qquad (6)$$

where $\lambda_{\pm}(x)$are the nonzero eigenvalues of the 3 × 3 reaction matrix. These eigenvalues are rate constants for the faster and slower phases of recovery for a single head, before strain-averaging as specified by the integral. The eigenvalues and coefficient functions $C_{\pm}(x)$ are version-dependent, and Eq. 6 requires a separate derivation in each case. Specific formulae are given in the Appendix.

Numerical calculations were made by setting $P(x) = 1$. Because the range of strains involved in the response increases with the size of the step, this procedure should be correct for small step perturbations. Although absolute amplitudes of tension recovery cannot be predicted without prior knowledge of $P(x)$, fractional amplitudes of recovery in each phase can be computed and compared with experimental data.

Version *A* is defined by the reaction scheme

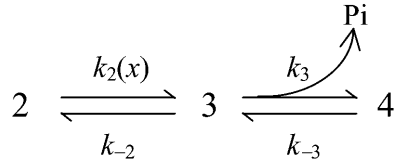

SCHEME 3

with a modest rate $k_3$of Pi release. We assume that the strain-dependence of the force-generating step is in the forward rate, and the Pi-release step is strain-independent. Tension is kx in the prestroke state 2 and $k(x + h)$ in the poststroke states 3, 4. The state probabilities $p_j(x,t)$ (j = 2,3,4) satisfy coupled rate equations, and their sum $P(x)$ is conserved in time. The strain-averaged tension response to a general step perturbation is

$$\Delta T(t) = \frac{k}{b}\int \{x\Delta p_2(x,t) + (x+h)(\Delta p_3(x,t) + \Delta p_4(x,t))\}dx, \qquad (7)$$

where the $\Delta p_j(x,t)$ (j = 2,3,4) are deviations from the final equilibrium defined by the model. In the Appendix, these deviations are expanded in terms of the exponentials $\exp(-\lambda_{\pm}(x)t)$, so that the coefficients are determined from their initial values $\Delta p_j(x,0)$. For this version,

$$\lambda_{\pm}(x) = \frac{1}{2}\{r_2(x) + r_3 \pm \sqrt{(r_2(x) - r_3)^2 + 4k_{-2}k_3}\}, \quad (8)$$

where $r_3 = k_3 + k_{-3}$, and the rate of stroke reversal is assumed to be strain-independent.

The strain-dependence of these eigenvalues is shown in Fig. 3 *A*. Both are decreasing functions of x, because $k_2(x)$ is a decreasing function. For a given strain, both rates increase with k_{-3} and therefore with the concentration [Pi] of free phosphate. The faster rate is a weakly increasing function and remains fast ($> k_{-2}$) in the absence of Pi ($k_{-3} = 0$). However, the slower rate is strongly phosphate-dependent. For large negative strains ($x \ll x_*$), the slower rate is equal to r_3, which implies that the process involved is the Pi-release transition in isolation from force generation, which is in rapid equilibrium and biased strongly toward state 3 ($K_2(x) \gg 1$). The slower rate is more strongly Pi-dependent at large positive strains ($x \gg x_*$) and slows to zero as [Pi]$\rightarrow$0, which implies that phosphate binding is followed by an irreversible backward stroke ($3 \rightarrow 2$ with $K_2(x) \ll 1$), which short-circuits any release of Pi from state 3. These statements can be confirmed from the eigenvectors of the reaction matrix (Eq. A1), which show the states involved in each phase for a given strain.

The coefficient functions $C_{\pm}(x)$ depend on the kind of step perturbation, and Eq. A2 gives a general formula in terms of initial state probabilities. However, predicted rates of recovery can be understood without this level of detail by considering the amount of strain-averaging required for a particular step. First, the critical strain separating pre- and poststroke states in equilibrium is not x_* but x_P, where $K_2(x_P)(1 + K_3) = 1$. Thus

$$x_P([\mathrm{Pi}]) = x_* + \gamma^{-1}\ln(1 + \tilde{K}_3/[\mathrm{Pi}]), \quad (9)$$

which decreases logarithmically with added phosphate. The following statements are true in the box approximation: i), After a length step Δl, the range of x values of responding heads is $(x_P, x_P + \Delta l)$. And ii), after a phosphate jump, the response is driven solely by the change in critical strain, say from an initial value x_{P0} to a final value x_P; the range of strains involved is just (x_{P0}, x_P). Thus, observed recovery rates are a weighted average (technically a cumulant average) of the eigenvalues over the range of x defined by the perturbation.

The phosphate dependence of x_P is also responsible for the logarithmic decrease of isometric tension over a wide range of Pi concentrations (Millar and Homsher, 1992; Tesi et al., 2000), although an exact formula must include a decrease in the bound fraction, and hence muscle stiffness, with increasing [Pi]. Although $P(x)$ depends weakly on the initial phosphate level, it should not change during rapid recovery from a phosphate jump.

Version *B* of the general model has a slow transition before force generation, after which Pi is released very rapidly and reversibly. A model of this kind has been proposed by Gutfreund and Ranatunga (1999). The post-stroke states A.M.ADP.Pi and A.M.ADP states are in rapid equilibrium and can be lumped together in state 3, giving the reaction scheme

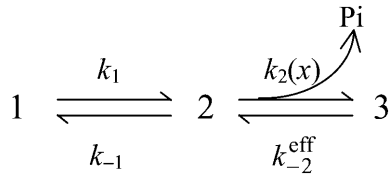

SCHEME 4

where $k_{-2}^{\mathrm{eff}} = k_{-2}/(1 + K_3)$. As in version *A*, $K_3 \equiv \tilde{K}_3/[\mathrm{Pi}])$ is the first-order equilibrium constant for Pi release. The tension transient is

$$\Delta T(t) = \frac{k}{b}\int \{x(\Delta p_1(x,t) + \Delta p_2(x,t)) + (x+h)\Delta p_3(x,t)\}dx, \quad (10)$$

which also leads to Eq. 6, but with a different formula for the coefficients (Eq. A4).

The eigenvalues are given by a formula isomorphous to Eq. 8,

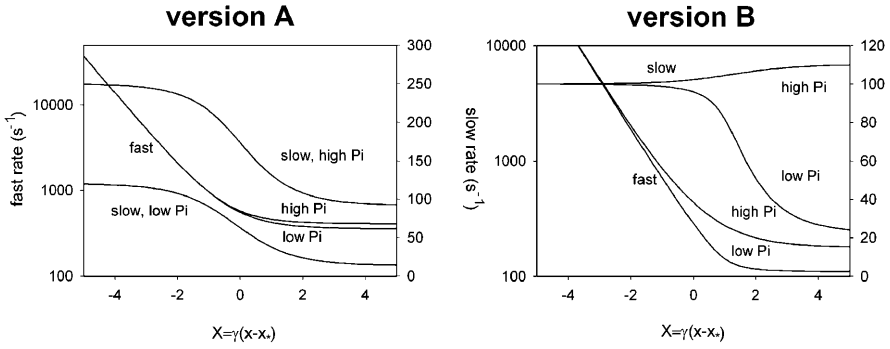

FIGURE 3 Rates of the faster and slower phases (the eigenvalues of Eqs. 8 and 11) versus reduced strain $X \equiv \gamma(x - x_*)$ in versions *A* and *B* of the three-state model with $k_{-2} = 250\,\mathrm{s}^{-1}$. (*Version A*) $k_3 = 100\,\mathrm{s}^{-1}$ and $k_{-3} = 20\,\mathrm{s}^{-1}$ or $150\,\mathrm{s}^{-1}$ for 1 mM or 25 mM [Pi], respectively. Both rates always increase with phosphate and decrease with step size. (*Version B*) $k_1 = 100\,\mathrm{s}^{-1}$, $k_{-1} = 10\,\mathrm{s}^{-1}$, and $K_3 = 10$ and 0.4 at low and high Pi as above. The slower rate increases with step size when $k_1 < k_{-2}/(1 + K_3)$. This condition is met at high phosphate ($K_3 < 1.5$, [Pi] > 6.7 mM).

$$\lambda_{\pm}(x) = \frac{1}{2}\{r_1 + r_2(x) \pm \sqrt{(r_1 - r_2(x))^2 + 4k_{-1}k_2(x)}\}, \tag{11}$$

with $r_1 = k_1 + k_{-1}$, $r_2(x) = k_2(x) + k_{-2}^{\text{eff}}$. Fig. 3 *B* shows that their behavior is qualitatively similar to those of version *A*, except that at high Pi the slower eigenvalue increases slightly with strain. For large negative strains, the rate of the slower phase is equal to k_1, because the slow transition $1 \rightarrow 2$ is coupled to an irreversible working stroke that short-circuits the return transition $2 \rightarrow 1$. For large positive strains, $k_2(x) \rightarrow 0$ and the two phases are produced by the separate transitions of the model; the faster and slower rates are, respectively, the larger and smaller of k_{-2}^{eff} and r_1. The consequences are interesting because k_{-2}^{eff} is Pi-dependent. At large +ve strains and low Pi, the slower rate is equal to k_{-2}^{eff}, which tends to zero at zero [Pi]; thus at low Pi the slower rate is a decreasing function of strain. At higher levels of Pi such that $k_{-2}^{\text{eff}} > k_1$, the slower rate becomes an increasing function, asymptoting to r_1 in the limit of large +ve strain and high Pi.

Note that the critical strain x_{P} is such that $K_1K_2(x_{\text{P}})(1 + K_3) = 1 + K_1$. This quantity is given by a modification of Eq. 9, in which the term $\gamma^{-1}\ln(K_1/(1 + K_1))$ is added to the right-hand side, and decreases in the same way with added phosphate.

A model with Pi release before force generation

A model in which Pi is released slowly before force generation has also been investigated. The kinetic scheme is

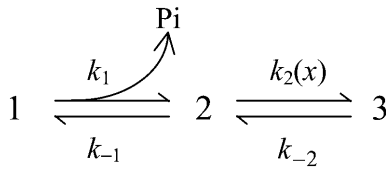

SCHEME 5

where the second transition generates tension as previously. The eigenvalues have the form of Eq. 11, where $k_{\pm 1}$ are now associated with Pi release. In this case, the slower eigenvalue is an increasing function of strain when $k_{-2} > k_1$, which is a defining condition of the model independent of Pi concentration. This property will be reflected in the rate of the slower phase of recovery from a length step, according to the range of strains sampled. However, at low Pi the observed rate of slower recovery is a decreasing function of step size (Ranatunga et al., 2002). Thus this model can be ruled out for striated muscle.

PHOSPHATE-DEPENDENT RESPONSE TO LENGTH STEPS

Strong evidence for the kinetic coupling of tension generation and phosphate release is provided by the phosphate dependence of tension recovery to length steps of different sizes (Ranatunga et al., 2002). Their data show two phases of recovery, which can be regarded as subphases of phase 2 (Davis and Rodgers, 1995). The existence of two phases shows that a slow step separate from force generation is required. For a given step, the rate of the faster phase is little affected by phosphate, whereas that of the slower phase is markedly phosphate-dependent for stretches but not for releases. The rates of both phases are decreasing functions of step size Δl, which requires the model with Pi release after force generation.

Tension responses from both versions of this model were calculated from Eq. 6, with coefficient functions from Eq. A6 (version *A*) or Eq. A8 (version *B*). These formulae were derived with the ''box'' approximation, in which the response comes from heads with strains between x_{P} and $x_{\text{P}} + \Delta l$. In this range, $P(x)$ is assumed constant.

The nature of the responses is shown in Figs. 4 and 5. Rate constants have been chosen to approximate experimental data. In each version, the forward rate of the slow transition was set at 100 s^{-1}, and $k_{-2} = 250\ s^{-1}$ unless stated otherwise. The equilibrium constant for Pi release should be 5–10 mM to fit the observed hyperbolic Pi dependence of the rate of the slower phase (Fig. 3).

Version *A* was explored with $k_3 = 100\ s^{-1}$ and $k_{-3} = 20\ s^{-1}$ at 1mM Pi. The faster phase is dominant in release and the slower phase in stretch. For releases, the faster rate is approximately proportional to $\exp(-\eta\gamma\Delta l)$, where $\eta = 0.37$, as predicted by the two-state model. The results in Fig. 4 *A* mimic rates of faster and slower recovery observed by Ranatunga et al. (2002) for rabbit psoas muscle at 1 mM Pi, except that for the faster rate in release, asymptotic to $\exp(-\gamma_{\text{eff}}\Delta l)$, their values of γ_{eff} (0.09–0.16 nm^{-1}) are much lower than found in frog muscle ($0.37 \times 1.2 = 0.44\ nm^{-1}$). This discrepancy suggests that the submillisecond responses expected from 5–10 nm releases can be obscured by extraneous elastic compliances, making it difficult to extract a meaningful value of γ. For stretches, their data are consistent with a flatter curve, as predicted by version *A*.

Recovery at 25 mM Pi was modeled with a Pi-binding rate of 150 s^{-1}, consistent with the assumption that Pi binding is a two-step process for which k_{-3} is a hyperbolic function of [Pi] (Michaelis-Menten kinetics). For stretches and releases, the rate of the faster phase increases weakly with k_{-3}. However, the slower rate is an approximately hyperbolic function of k_{-3} (Fig. 5 *A*), starting from zero and saturating at high values; the value of k_{-3} for half saturation and the saturation rate are both decreasing functions of step size. These findings are generally consistent with the observations of Ranatunga et al., but the predicted increase of the slower rate with [Pi] in release is not observed. However, the fractional amplitude of the slow phase in release is small, and their standard errors for this rate are understandably large.

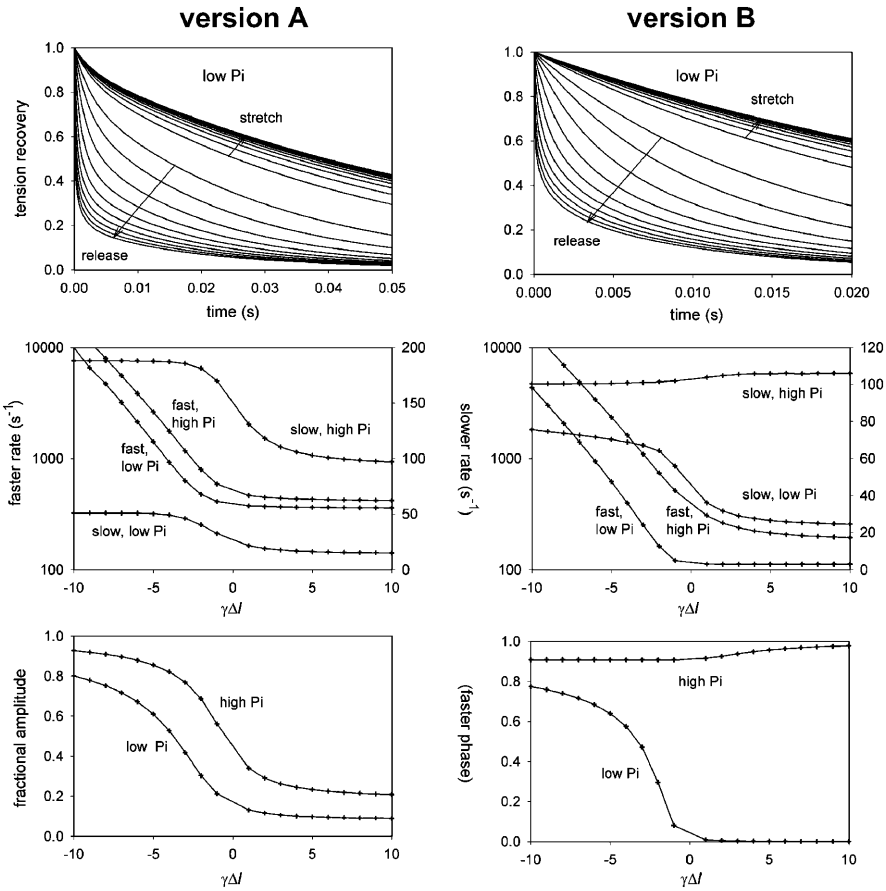

FIGURE 4 Biphasic tension recovery from a length step in the two versions of the three-state model, showing, from top to bottom: i), tension recovery at low Pi for 10 different stretches and releases as in Fig. 2 *A*; ii), rates of the faster phase (logarithmic left-hand vertical scale) and slower phase (right-hand vertical scale) versus reduced step size $\gamma\Delta l$ at low and high Pi; and iii), the fractional amplitude of the fast phase versus step size.

The predicted fractional amplitudes of the phases are very sensitive to step size. Ratios of experimental amplitudes follow the same trends, but the variation with step size is less extreme; for example, at low Pi the fractional amplitude of the faster phase varies from 0.75–0.8 for a 5 nm release to 0.5 for a 5 nm stretch) After stretch, this fraction increases significantly at high Pi as predicted, though at low Pi an equal mixture of phases is observed, rather than the dominant slower phase predicted by the model. These discrepancies could be an artifact of fitting the data to two exponentials; this process is avoided in the modeling, which predicts the (generally nonexponential) time course of each phase. Alternatively, isometric tension may include contributions from a second A.M.ADP state, which is not included in the model.

With $k_3 = 100\text{s}^{-1}$, the behavior of the model as a function of k_{-2} is summarized in Table 1. Larger values of k_{-2} increase the rate and amplitude of fast recovery overall, and the rate of slow recovery at high Pi only. If Pi release is made more irreversible by reducing the value of k_{-3}, the rate of the slow phase in stretch is reduced as expected, but the amplitude of the slow phase increases and may become dominant even for small releases.

Version *B* was explored similarly, with $k_1 = 100\ \text{s}^{-1}$and $\tilde{K}_3 = 10\text{mM}$ for the second-order phosphate-release constant. The release of phosphate is rapid and reversible, so Pi concentration enters only through the first-order dissociation constant $K_3 = \tilde{K}_3/[\text{Pi}]$. This version has a fourth parameter k_{-1}, and Figs. 4 *B* and 5 *B* show the behavior predicted with $k_{-1} = 10\ \text{s}^{-1}$. The above value of $\tilde{K}_3$ causes the rate of the slower phase to saturate at high Pi as observed. However, the rate of the faster phase for small steps is only 100–200 s^{-1}, which is a factor of 4 lower than observed in rabbit and frog muscle.

Table 2 summarizes the predictions of this version as a function of k_{-2}. As expected, the rate of the faster phase increases with k_{-2}, but the characteristic decrease in the rate of the slower phase with step size is progressively reduced, and replaced by an increase when $k_{-2} > (1 + K_3)k_1$. This occurs first at high Pi where $K_3 \gg 1$, and eventually at low Pi also, which is not observed experimentally. It appears that version *B* cannot be fine-tuned to match both these properties to experiment.

Comparisons show that the two versions of the model give qualitatively similar length-step predictions but differ in detail. For the parameters used, version *B* differs in the following respects: i), at low Pi, the rate of the faster phase after a small step is reduced from 390 to 120 s^{-1}, whereas a rate of ~500 s^{-1} is observed in rabbit at 10°C (Ranatunga et al., 2002; Kawai, 1986); ii), at high Pi, the rate of the slower phase increases with step size; iii), for a large release, the rate of the slower phase varies less with [Pi]; and iv), at

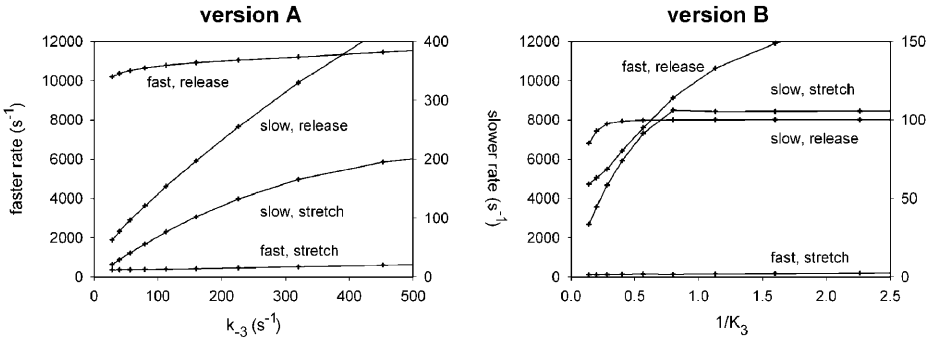

FIGURE 5 Phosphate dependence of the rate constants shown in Fig. 4, for a large stretch ($\gamma\Delta l = 10$) and large release ($\gamma\Delta l = -10$). Phosphate concentration is represented by the rate of binding k_{-3} (say 20 s^{-1} for 1 mM Pi) in version *A*, or the binding constant $1/K_3$ (say 0.1 at 1 mM Pi) in version *B*. Values of kinetic parameters are given under Fig. 3.

high Pi, the fast phase is dominant after a large stretch. The accuracy of the rate data is insufficient to rule out point ii, particularly as version *B* gives only a small increase with step size when $k_{-1} \ll k_1$. Point iii is apparently confirmed by Ranatunga et al., but with large errors in a region where the phase amplitude is small. With respect to point iv, neither version really accounts for the observed amplitudes of the phases. Thus the existing data do not discriminate between the two versions, except on numerical grounds arising from point i. Although the numerical discrepancy in point i can be removed by increasing the value of k_{-2}, Table 2 shows that this improvement can only be obtained at the expense of point ii.

We conclude that observed biphasic recovery from length steps is slightly better described by version *A*, which can be characterized as follows. At low Pi, the rate of the slower recovery phase decreases by a factor of ~4 from release to stretch. At high Pi, the rate of the slower phase also decreases with step size but the decrease is much less pronounced. Rates of the faster phase stay well above rates of the slower phase for the same or any other step size. Increasing levels of Pi accelerate the slower phase for stretches only, the rate of the faster phase increasing only slightly. Finally, note that the two versions do give qualitatively different predictions for the step-dependence of the rate of the slower phase at high Pi.

TABLE 1 Indicators of the length-step behavior of model version *A* as a function of k_{-2} for k_3 = 100 s^{-1}

k_{-2} (s^{-1})	$r_+(0)$ (s^{-1})	η	$r_-(-10)$ (s^{-1})	$r_-(+10)$ (s^{-1})	$\gamma\Delta l_c$
100	220	0.35	41.9	10.3	−4.8
	322	0.43	147	53.9	−2.7
250	393	0.37	51.0	15.1	−3.8
	527	0.44	188	97.1	−0.45
500	689	0.38	55.0	17.7	−3.3
	932	0.44	202	124	+1.6

In each row, upper and lower entries were generated with $k_{-3} = 20$ and 150 s^{-1}, representing 1 mM and 25 mM Pi, respectively. $r_+(0)$ is the rate of the faster phase for small steps, and η the logarithmic slope for large releases where the rate is proportional to $\exp(-\eta\gamma\Delta l)$. $r_-(-10)$ and $r_-(10)$ are rates of the slower phase for a large release and stretch, respectively ($\gamma\Delta l = \mp 10$). $\gamma\Delta l_c$ is the reduced step size for which the amplitudes of each phase are equal; for steps smaller than this, the faster phase has the larger amplitude, and vice versa.

PHOSPHATE JUMPS

Caged-Pi experiments

The tension response to flash photolysis of caged Pi in a skinned muscle fiber has been measured by Millar and Homsher (1990) and Dantzig et al. (1992). The response consists of a lag of a few milliseconds (phase 1), followed by an exponential fall (phase 2) and a slower approach to the final steady state (phase 3). This behavior appears to conflict with the models of the previous section, which predict a biphasic response. In fact, a lag is predicted by models in which the faster phase causes an increase in tension. We have chosen to fit observed rate constants for phase 2 as a function of final Pi concentration by the hyperbolic function

$$r([\mathrm{Pi}]) = \frac{\alpha[\mathrm{Pi}]}{[\mathrm{Pi}] + \beta}, \tag{12}$$

which passes through the origin (Fig. 6). The data appear to lie above the fitted curve at low Pi and below at intermediate concentrations, and better fits can be obtained by a three-parameter function with a finite rate at zero phosphate. However, fitting to Eq. 12 is a useful intermediate step in

TABLE 2 Length-step indicators of model version *B*, as a function of k_{-2} and k_{-1}, for k_1=100s^{-1} and K_3= 10 mM

k_{-2} (s^{-1})	k_{-1} (s^{-1})	$r_+(0)$ (s^{-1})	η	$r_-(-10)$ (s^{-1})	$r_-(10)$ (s^{-1})	ρ_+ (−10)	ρ_+ (10)
100	10	112	0.39	49.2	9.85	0.68	0.0001
		180	0.47	99.2	74.1	0.89	0.071
	100	213	0.41	65.5	9.81	0.35	0.0003
		356	0.49	98.0	73.4	0.47	0.028
250	10	117	0.46	75.6	24.6	0.77	0.0013
		411	0.47	100	106	0.91	0.98
	100	239	0.48	83.2	24.3	0.40	0.0024
		672	0.49	102	165	0.50	0.22
500	10	139	0.47	94.6	48.6	0.86	0.014
		813	0.46	100	107	0.91	0.99
	100	289	0.49	93.6	47.8	0.44	0.011
		1240	0.48	103	156	0.51	0.89

Upper and lower entries in each row are for 1 and 25 mM Pi (K_3 = 10 and 0.4), respectively. ρ_+ is the fractional amplitude of the faster phase; other quantities are defined in Table 1. In this model, r_- at high Pi increases with step size in the last four rows, where $k_{-2} > (1 + K_3)k_1$; under these conditions the faster phase generally predominates in stretch.

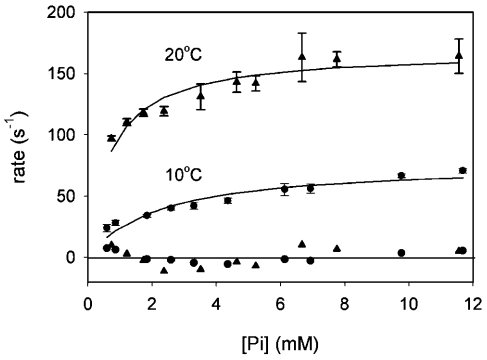

FIGURE 6 Measured rates of tension change after photo release of caged Pi as a function of final Pi concentration (Dantzig et al., 1992; coordinates and standard errors supplied by courtesy of J. Dantzig), fitted to hyperbolic functions passing through the origin (Eq. 12). Unweighted least-squares fitting gives $\alpha = 78\pm6\ s^{-1}$, $\beta = 2.18\pm0.05$ mM at 10°C, and $\alpha = 168\pm6\ s^{-1}$, $\beta = 0.69\pm0.13$ mM at 20°C. For the 10°C data, error-weighted fitting gives similar results. Residuals as shown are positive at low Pi.

matching the data to predicted rate curves as functions of k_{-3} or $1/K_3$.

As discussed, strain-dependent three-state models give a theoretical framework for understanding phosphate-jump responses. An upward phosphate jump alters the critical strain separating heads in equilibrated prestroke and poststroke states, from x_{P0} to a lower value x_P. The variation of response rate with final Pi concentration can be understood as an average of the slower eigenvalue of Fig. 3 over the range (x_P, x_{P0}), which always lies to the right of x_* (Eq. 9). Thus the predicted response rate increases with final [Pi] as x_P falls. Moreover, the response rate falls to zero when initial and final Pi concentrations both tend to zero. However, this description assumes that the slower phase is dominant for Pi jumps. Calculations were carried out only for the model with Pi released after force generation.

In version *A*, a sudden excess of free Pi increases the population of heads in the poststroke A.M.ADP.Pi state without tension change; the observed drop in tension is produced by the subsequent reversal of the working stroke. The rate of tension change will be limited by Pi binding, which in this version is slower than the rate of force reversal, and the fast phase is driven by the effects of the slow phase and so is largely silent. Note that the unaveraged rate indicated by the slower phase in Fig. 3 *A* is closer to k_{-3} than r_3, because the reversal of the working stroke is faster than phosphate release, and hence becomes very small in the limit of zero final [Pi].

In version *B*, Pi binding is rapid and the rate of tension change is controlled by the effective rate $k_{-2}/(1 + K_3)$ of stroke reversal $(K_3 \equiv \tilde{K}_3/[\mathrm{Pi}])$, which is independent of strain and has a hyperbolic dependence on final Pi concentration. The kinetic scheme is such that no lag in tension response is expected. Although no intrinsic change in tension is associated with the prestroke transition, a slower component of tension response is generated as the transition $2 \rightarrow 1$ drives the overall equilibrium toward prestroke states.

Fig. 7 shows the responses calculated from Eq. 6 and Eqs. A10 or A11 for various phosphate jumps, starting from a nominal level of 1 mM Pi. Empirical rates of change are calculated to 1/e of the total change as previously, and the bottom panels show the effects of varying the value of k_{-2}.

For version *A*, the predicted tension change is biphasic; the empirical rate reflects the slower phase of the model, and the faster phase is manifested as a lag as observed. The empirical rate increases with final [Pi] as measured by k_{-3}, asymptoting to a value of the order of k_{-2} at high concentrations beyond the range of the experiment. The time courses of each phase (not shown) reveal that the lag is generated by the faster phase in which tension increases; with increasing [Pi], the fractional amplitude of this phase changes from -0.05 to -0.6, and its rate from 400 to 600 s^{-1}. The corresponding lag times (2.5–1.7 ms) are close to those observed by Dantzig et al. (2.1–1.8 ms for 1–6 mM Pi). The responses are insensitive to the value of k_3, and lower values as found by White et al. (1997) can also be used.

In version *B*, the empirical rate constant also increases with [Pi] as measured by the binding constant $1/K_3$, and asymptotes to r_1. For the rate constants used, the transients are generally faster than in version *A* for the same value of k_{-2}. In this version there is no lag phase; the fractional amplitudes of both phases are positive, and there is a gradual transfer of amplitude from the slower phase to the faster phase with increasing [Pi].

On this basis, version *A* is preferred over version *B* as it does show a lag phase as observed, and does not generate an excessively fast transient for values of k_{-2} ($\sim$250 s^{-1}) that fit length-step data.

In principle, predicted rate curves could be fitted to the data in Fig. 6 by using Eq. 12 as an intermediary. However, the predicted curves are functions of k_{-3} or $1/K_3 \equiv [\mathrm{Pi}]/\tilde{K}_3$, and the data are a function of Pi concentration. Quantitative tests of the two versions are possible only if k_{-3} is a known function of [Pi] and the value of $\tilde{K}_3$ is known; unfortunately, these quantities are not well-characterized experimentally. Thus the following curve-fitting procedures should be viewed as a method for extracting this information.

The rate curves in Fig. 7 can be approximated by hyperbolic functions of the independent variable, say

$$r(k_{-3}) = a_3 k_{-3}/(k_{-3} + b_3) \tag{13A}$$

$$r(K_{-3}) = A_3 K_3^{-1}/(K_3^{-1} + B_3) \tag{13B}$$

for versions *A* and *B*, respectively, which pass through the origin. The figure shows that the fitted curve lies slightly below calculated coordinates near the origin and above them at large values of the argument, for reasons to be explained shortly. However, the deviations are not as large as in Fig. 6.

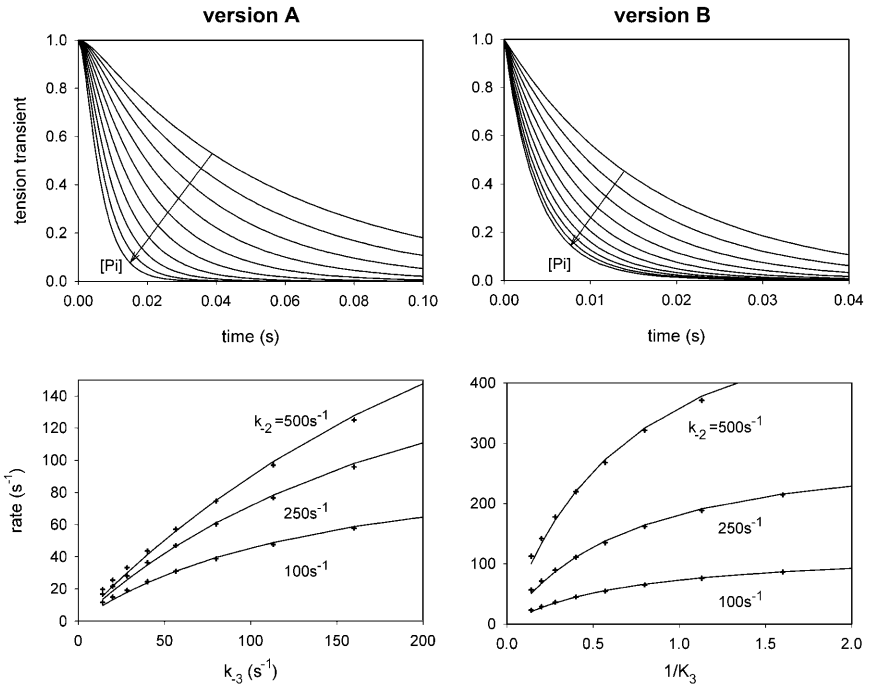

FIGURE 7 Predictions of versions *A* and *B* for caged-Pi experiments, for 10 upward phosphate jumps from nominally 1 mM Pi, generated by increasing the rate of Pi binding k_{-3} (*A*) or Pi affinity $1/K_3$ (*B*) by successive powers of $\sqrt{2}$. Values of all other rate constants are given under Fig. 3. (*Upper panels*) Tension transients, normalized to the total change after equilibration. The slower phase is predominant (see main text). (*Lower panels*) Empirical rates of change (to 1/e = 0.37) versus final [Pi] as measured by k_{-3} or $1/K_3$, with various values of k_{-2}. Computed coordinates are shown as crosses, and the lines are fitted hyperbolic functions (Eqs. 13A or 13B). For version *A*, $a_3 = 115\pm4$, 247 ± 11, and 423 ± 24 s^{-1}; $b_3 = 152\pm10$, 243 ± 18, and 369 ± 32 s^{-1} in increasing order of k_{-2}. For version *B*, $A_3 = 127\pm2$, 314 ± 5, and 622 ± 11 s^{-1} similarly, whereas $B_3 = 0.73\pm0.03$ throughout.

For version *A*, the data cannot be fitted if k_{-3} is linear in [Pi], and a Michaelis-Menten function is required, say

$$k_{-3}([\mathrm{Pi}]) = \frac{V_3[\mathrm{Pi}]}{[\mathrm{Pi}] + C_3}. \tag{14}$$

Now a hyperbolic function of a hyperbolic function is also a hyperbolic function; substitution in Eq. 13 A leads back to Eq. 12 with $\alpha = a_3V_3/(V_3 + b_3)$, $\beta = b_3C_3/(V_3 + b_3)$. Hence any predicted hyperbolic rate curve can be matched to the data by using the Michaelis-Menten constants

$$V_3 = \frac{\alpha b_3}{a_3 - \alpha}, \quad C_3 = \frac{\beta a_3}{a_3 - \alpha} \tag{15}$$

as long as $a_3 > \alpha$. In this case, the caged-Pi data provide no quantitative test of version *A* unless appropriate values of C_3 and/or V_3 are known in advance: all three rate curves in Fig. 7 *A* can be fitted to experiment. With $k_{-2} = 250$ s^{-1}, the predicted curve matches the 10°C data if $V_3 = 111$ s^{-1} and $C_3 = 3.17$ mM. The predicted value of the second-order Pi-release constant $\tilde{K}_3 = k_3C_3/V_3$ is 2.87 mM. Other values of k_{-2} are accommodated by making opposing changes in V_3 and C_3.

Version *B* allows a slightly more meaningful test, since it predicts the rate of tension fall as a function of $1/K_3 \equiv [\mathrm{Pi}]/\tilde{K}_3$, with only one unknown constant. The rate curves in Fig. 7 *B* are well-fitted by Eq. 13B, and are matched to data fitted by Eq. 12 if

$$\alpha = A_3, \quad \beta = B_3\tilde{K}_3. \tag{16}$$

The first equation tests the model, and the second equation gives the value of $\tilde{K}_3$. All three curves require $\tilde{K}_3 = 3.00$mM to match the data at 10°C and 0.94 mM for the data at 20°C. The best-fit value of A_3 is approximately proportional to k_{-2}. However, very low values of k_{-2} (61 s^{-1} at 10°C, 133 s^{-1} at 20°C), about fourfold smaller than needed for length-step data, are required to match the experimental values of α given under Fig. 6. In this sense, data-fitting confirms that version *A* gives a better description of the caged-Pi data.

All Pi-jump calculations were made with the same initial concentration (nominally 1 mM) and a range of final concentrations. If the initial concentration were raised, the rate of change could be estimated by starting from an intermediate point on the curve. However, this procedure is not exact; the predicted rates then lie above the original curve. Similarly, a Pi jump from an initial state with almost no phosphate should give a rate curve below that observed by Dantzig et al., where initial [Pi] was ~1mM. These effects, and the systematic deviations from hyperbolic rate curves in Fig. 7, are produced by the non-exponential character of each phase of the transient response.

Version *B* is similar to the model proposed by Dantzig et al., in which phosphate is released rapidly after force generation. However, their model does not contain a slow transition before force generation, and the prestroke state was assumed to be strain-free. To fit their data, the Dantzig et al. model required a rate of 100 s^{-1} for reversing the force-generating transition.

Phosphate jumping up and down

By exchanging solutions in a micropipette with myofibrils, Tesi et al. (2000) observed that phosphate jumps in opposite directions to the same final Pi concentration (0.1 mM→5 mM and 10→5 mM) give different rates of tension change, faster by a factor of 4 for upward jumps relative to downward ones. Such effects can be expected when the tension transient is a continuous distribution of exponential decays, since the distribution of amplitudes would be determined by the initial state. This aspect of phosphate jumps appears to be a natural consequence of strain-dependent kinetics, just as stretches and releases of the same size give different rates of phase-2 recovery when the filaments remain in full overlap. What behavior is expected from mechanokinetic models?

Unfortunately, both versions of the three-state model used in this article generate a kinetic asymmetry in the opposite direction. Table 3 gives empirical rate constants (to 1/e) computed for a variety of jumps to the same final concentration, nominally 5 mM Pi, starting from Pi concentrations of 0.1, 1, 10, and 25 mM; the response is faster for downward than upward jumps. This property arises when the smaller eigenvalue of the kinetics (Fig. 3) is a decreasing function of strain; the empirical rate can be regarded as an average of this function over the range (x_P, x_{P0}). For upward jumps, $x_{P0} > x_P$. For downward jumps to the same final state, x_P is unchanged but $x_{P0} < x_P$, which samples heads at lower strain where the eigenvalue is bigger. This prediction would be reversed if $\lambda_-(x)$ were an increasing function of strain, which occurs in version *B* at high phosphate and/or high values of k_{-2} (Table 2). To fit the observations of Tesi et al., it would be necessary for the eigenvalue to increase with strain at all phosphate levels used, for example the rejected model in which phosphate is released before force generation. In that case, the slow rate of length-step recovery would increase with step size, which is clearly not observed by Ranatunga et al. (2002) at 1 mM Pi. It appears that these two experiments yield rate data that cannot be interpreted in terms of the same mechanokinetic model with force generation coupled to release phosphate. Perhaps a sequestering agent is slowing the removal of excess phosphate from myofibrils in the solution-mixing experiment.

TABLE 3 Empirical recovery rates predicted for upward and downward phosphate jumps to the same final concentration (nominally 5 mM), starting from lower and higher concentrations

Version *A*				
k_{-3} (s^{-1}) initial	k_{-3}(s^{-1}) final	X_{P0}	X_P	rate (s^{-1})
1	50	4.62	1.10	36.8
10		2.40		43.0
100		0.69		54.9
250		0.34		58.5
Version *B*				
$1/K_3$ initial	$1/K_3$ final	X_{P0}	X_P	rate (s^{-1})
0.01	0.5	4.52	1.00	103
0.1		2.30		126
1		0.60		179
2.5		0.24		199

Concentrations are entered as values of the Pi binding rate k_{-3}(version *A*) or Pi binding constant $1/K_3$ (version *B*). In all cases, the rate of recovery depends on the initial concentration and is greater for downward than upward jumps, reflecting the range of strains in the window (x_P, x_{P0}), where $X_P \equiv \gamma(x_P - x_*)$, $X_{P0} \equiv \gamma(x_{P0} - x_*)$.

DISCUSSION

By applying different kinetic models to length-step data at different phosphate levels, we have confirmed the long-standing proposal that the working stroke precedes the release of phosphate in the muscle cross-bridge cycle. After a similar analysis of caged-Pi data, we also conclude that the release of phosphate must be slower than the characteristic rate (k_{-2}) of force-generation (version *A*). This bound-state model is valid only if it can be embedded in the actin-myosin-ATP cycle so that rapid (phase 2) transient phenomena are generated by transitions internal to the model, whereas slower transients (phases 3 and 4) are caused by other transitions. As discussed below, the slow rate of Pi release and its reversibility at millimolar levels of Pi both force a reinterpretation of existing ideas about the cross-bridge cycle.

Slow Pi release after force generation

If Pi is released from the poststroke A.M.ADP.Pi state at 100 s^{-1}or less, this event may well be the rate-limiting step for product-release in the muscle fiber, so that the dominant poststroke state in activated muscle would not be A.M.ADP (Hibberd and Trentham, 1986; Pate and Cooke, 1989) but A.M.ADP.Pi. This suggestion is supported by observations of transient rates of Pi release in permeabilized fibers (He et al., 1997) and myofibrils (Lionne et al., 2002 and references therein), which show that there is no burst of free Pi under isometric or isotonic conditions. Isometric striated muscle exhibits high force (1–2 pN/head, Coupland et al., 2001; Ford et al., 1977) and low ATPase (1–6 s^{-1}, Hilber et al., 2001), whereas unloaded fast muscles shorten at high speed (2–10 μm/s, Cook et al., 1997; Cooke and Pate, 1995) with a faster turnover of ATP (Fenn, 1924; Huxley, 1957). Before the above observations of Pi release, it was thought that these effects could be accommodated if the rate of ADP release was under strain control, so that rates of detachment from tension-holding states are very low under isometric conditions, but much faster under unloaded shortening. Unloaded shortening velocity is estimated by the formula $v \sim gh$ for detachment rate g; thus $h = 10$ nm requires $g = 200$–1000 s^{-1}, comparable to rates of ADP release in solution (Siemankowski et al., 1985). Mechanisms

for strain control of ADP release have been proposed by Smith and Geeves (1995) and Duke (1999). Alternatively, a form of ''loose coupling'' has been suggested where bound heads under large compressive strain are forcibly detached from actin, to rapidly rebind to the same actin site or neighboring sites (Brenner 1991).

It should now be clear that a 100 s^{-1} rate of Pi release is incompatible with observed shortening speeds in fast fibers. Some form of strain control is required, so that Pi is released as above at zero or positive strain, but more rapidly at large negative strains. Now bound ADP can only be released through myosin's open nucleotide pocket, whereas bound Pi might also be released into the actin-binding cleft (Yount et al., 1995). It is tempting to speculate that this ''back door'' route might account for the rate of release seen under isometric conditions, and the faster ''front door'' route is blocked by positive strain.

A strain-dependent mechanism for Pi release is not part of the models presented here. Its inclusion would certainly modify our predictions for the rate of the slower recovery phase at negative strains (Fig. 3). This region is rather inaccessible to length-step experiments, as the amplitude of the slower phase (observed and predicted) is very small for large releases. Thus the model should still be competent to predict observable aspects of phase-2 recovery.

Reversibility of Pi release

The reversibility of Pi release in fibers required by modeling ($\tilde{K}_3 \approx 3$mM at 10°C) and the effects of millimolar phosphate on isometric tension (Millar and Homsher, 1992; Tesi et al., 2000), are in stark contrast to the difficulty of binding Pi to the A.M.ADP state prepared by binding M.ADP to actin (Sleep and Hutton, 1980). Such considerations led Sleep and Hutton to propose the existence of a precursor state (A.M′.ADP) on the pathway of the cross-bridge cycle. Solution kinetics suggests that the transition A.M′.ADP→A.M.ADP should be fast and moderately irreversible, with an equilibrium constant of ~100. If the rate of Pi release is strain-controlled as suggested, this isomerization would also need to be under strain control to make A.M′.ADP the dominant poststroke state in active muscle, accessible to millimolar levels of free phosphate. Myosin is a large protein; it would not be surprising if all product-release steps and the ATP binding step are accompanied by small working strokes and therefore affected by strain to some extent.

Limitations of bound-state models

To be meaningful, bound-state models for phase-2 transients should behave in the same way when embedded in an appropriate model of the actin-myosin-ATP cycle. This test is met if the complete model also generates the slower transient phases observed in various experiments; in this way it can be established that phases 3 and 4 of length-step recovery are generated by cycling heads (K. Burton, R. M. Simmons, and J. Sleep, unpublished; Chen and Brenner, 1993; Smith, 1998). For this article, a sufficient criterion is that rates of equilibration within the bound-state model (> 100 s^{-1}) should be faster than the rates of entry and exit. We have argued above that the exit rate from state 4 by release of ADP should be under 100 s^{-1}, at least under isometric conditions and after stretch. This appears to be confirmed by the characteristic rate 20–50 s^{-1} of anti-recovery in phase 3 (Lombardi et al., 1992), but there is some evidence that tension-holding states are forcibly detached by large stretches (Lombardi and Piazzesi, 1990; Piazzesi et al., 1997), and detachment is very rapid for stretches of 8 nm or more (Getz et al., 1998; Nishizaka et al., 2000). Thus our analysis of the slow component of phase-2 recovery, which dominates in stretch, is valid only for stretches below this threshold. Piazzesi et al. (1997) claim that heads are forcibly detached at 100 s^{-1} by a 4 nm stretch, which appears to conflict with the acceleration by phosphate of phase-2 *b* recovery from stretches.

There are various lines of evidence that the entry rate into state 1 by binding of M.ADP.Pi may be well above 100 s^{-1}. Solution kinetics suggests that strain-free heads in the muscle fiber should bind rapidly and reversibly to actin (Geeves, 1992), and this is confirmed by the reduction in fiber stiffness during the phase-2 response to a phosphate jump (Dantzig et al., 1992). If the detached state is in rapid equilibrium with the first bound state, it can be absorbed into the model and the rate of entry is controlled by the hydrolysis of M.ATP (Lymn and Taylor, 1971), typically 100 s^{-1}. This kind of model is required for the time course of force development after release of caged ATP (J. Sleep, M. Irving, and K. Burton, unpublished). However, if myosin can bind to several sites in a target zone on F-actin, the detached state is shared between these sites and the theory should be modified accordingly.

Finally, we have assumed that the elastic compliance of active muscle resides entirely in the bound heads, which is known to be incorrect. It can be shown that the shape of the T_2 curve for length-step recovery is very sensitive to filament compliance. However, the shape of the corresponding rate curve is less affected and given approximately by a rigid-filament model with k interpreted as the stiffness of a bound myosin and filaments in series. The tension transient from a phosphate jump occurs under nominally isometric conditions and should be less affected by filament compliance. To validate our models, a systematic study of the effects of elastic compliance in the filaments is desirable; this work is in progress.

CONCLUSIONS

We have shown that known effects of phosphate on tension transients after a length step or phosphate jump can be

explained if Pi is released slowly after a strain-dependent working stroke. The resulting cross-bridge cycle makes A.M.ADP.Pi a major tension-holding state in isometric striated muscle. These findings are relevant to current thinking about myosin structure. With new evidence that the actin-binding cleft of myosin 2 is closed in rigor (Conibear et al., 2003; Holmes et al., 2003; Reubold et al., 2003), it has been suggested that the transition from weak to strong binding and the working stroke are controlled by separate structural elements (switch 1 and switch 2). If so, our modeling results require that phosphate be released after switch 2 opens. It is plausible that switch 1 opens first, so that force generation and Pi release occur in strongly bound states. However, Houdusse and Sweeney (2001) have suggested that the working stroke and Pi release occur before the transition to strong binding, so that millimolar levels of phosphate can bind to the precursor form of A.M.ADP proposed by Sleep and Hutton (1980); the transition to strong binding could then be associated with the isomerization to the more stable form of A.M.ADP. This proposal is compatible with our model if both types of bound state are orientationally specific and can hold strain. The challenge is to find new protocols for muscle-fiber experiments to discriminate between these possibilities.

APPENDIX: RESPONSES IN THE FIRST THREE-STATE MODEL

Equations (A1–A4) below are independent of the kind of step perturbation, and provide a general solution to the kinetic equations of the model in terms of its eigenvalues. There are different forms for versions *A* and *B*, but in each case tension transients are calculated from Eq. 6 of the main text.

Version *A*

For the time courses of the changes in state populations,

$$\begin{pmatrix}\Delta p_2(x,t)\\ \Delta p_3(x,t)\\ \Delta p_4(x,t)\end{pmatrix}=\sum_{\pm}\frac{C_{\pm}(x)}{k_{-2}}\begin{pmatrix}-k_{-2}\\ \lambda_{\pm}(x)-k_2(x)\\ r_2(x)-\lambda_{\pm}(x)\end{pmatrix}\exp(-\lambda_{\pm}(x)t), \tag{A1}$$

whose sum is conserved at zero. (The column vector on the right-hand side is an unnormalized right eigenvector of the reaction matrix). On substituting in the rate equations for version *A*, we find that the coefficients $C_{\pm}(x)$ are determined by the initial values of these deviations:

$$\begin{aligned}C_+(x)&=\frac{\lambda_-(x)-k_2(x)}{\lambda_+(x)-\lambda_-(x)}\Delta p_2(x)+\frac{k_{-2}}{\lambda_+(x)-\lambda_-(x)}\Delta p_3(x),\\ C_-(x)&=\frac{k_2(x)-\lambda_+(x)}{\lambda_+(x)-\lambda_-(x)}\Delta p_2(x)-\frac{k_{-2}}{\lambda_+(x)-\lambda_-(x)}\Delta p_3(x).\end{aligned} \tag{A2}$$

Thus the tension transient can be computed if the initial deviations are known. These deviations must be calculated for a particular step perturbation from the isometric steady state, as shown below.

Version *B*

$$\begin{pmatrix}\Delta p_1(x,t)\\ \Delta p_2(x,t)\\ \Delta p_3(x,t)\end{pmatrix}=\sum_{\pm}\frac{C_{\pm}(x)}{k_2(x)}\begin{pmatrix}\lambda_{\pm}(x)-r_2(x)\\ k_{-2}^{\mathrm{eff}}-\lambda_{\pm}(x)\\ k_2(x)\end{pmatrix}\exp(-\lambda_{\pm}(x)t), \tag{A3}$$

where

$$\begin{aligned}C_+(x)=&\frac{-k_2(x)}{\lambda_+(x)-\lambda_-(x)}\Delta p_2(x)\\ &-\frac{\lambda_-(x)-k_{-2}^{\mathrm{eff}}}{\lambda_+(x)-\lambda_-(x)}\Delta p_3(x),\\ C_-(x)=&\frac{k_2(x)}{\lambda_+(x)-\lambda_-(x)}\Delta p_2(x)+\frac{\lambda_+(x)-k_{-2}^{\mathrm{eff}}}{\lambda_+(x)-\lambda_-(x)}\Delta p_3(x).\end{aligned} \tag{A4}$$

Length steps

Version A

By analogy with Eq. 2, the initial deviations from final equilibrium are

$$\begin{aligned}\Delta p_3(x)=&\left(\frac{K_2(x-\Delta l)}{1+K_2(x-\Delta l)(1+K_3)}-\frac{K_2(x)}{1+K_2(x)(1+K_3)}\right)\\ &P(x-\Delta l),\\ \Delta p_4(x)=&K_3\Delta p_3(x)\end{aligned} \tag{A5}$$

and their sum is $-\Delta p_2(x)$. In the box approximation, the bracketed quantity is equal to $1/(1+K_3)$, respectively, for all x in $(x_{\mathrm{P}}, x_{\mathrm{P}}+\Delta l)$ and zero outside, where x_{P} is given by Eq. 9 of the main text. Hence

$$C_{\pm}(x)=\pm\frac{k_2(x)+\frac{k_{-2}}{1+K_3}-\lambda_{\pm}(x)}{\lambda_+(x)-\lambda_-(x)}P(x-\Delta l) \tag{A6}$$

inside this range, and zero otherwise.

Version B

Analogous operations give

$$\begin{aligned}\Delta p_1(x)=&\left(\frac{1}{1+K_1+K_1K_2^{\mathrm{eff}}(x-\Delta l)}-\frac{1}{1+K_1+K_1K_2^{\mathrm{eff}}(x)}\right)\\ &P(x-\Delta l),\\ \Delta p_2(x)=&K_1\Delta p_1(x),\end{aligned} \tag{A7}$$

where $K_2^{\mathrm{eff}}(x)=K_2(x)(1+K_3)$. In the box approximation, the bracketed quantity equals $-1/(1+K_1)$ for x in $(x_{\mathrm{P}}, x_{\mathrm{P}}+\Delta l)$ and zero outside, where x_{P} is given by the modified form of Eq. 9 with the additional term $\gamma^{-1}\ln(K_1/(1+K_1))$. Then

$$C_{\pm}(x) = \pm\frac{\dfrac{K_1 k_2(x)}{1+K_1} + k_{-2}^{\text{eff}} - \lambda_{\mp}(x)}{\lambda_+(x) - \lambda_-(x)} P(x - \Delta l) \qquad \text{(A8)}$$

in this range, and zero outside it.

Phosphate jumps

Version A

Let K_{30}, K_3 be first-order equilibrium constants for the Pi release step at the initial and final phosphate levels. The initial deviations are

$$\Delta p_2(x) = \left(\frac{1}{1+K_2(x)(1+K_{30})} - \frac{1}{1+K_2(x)(1+K_3)}\right)P(x),$$
$$\Delta p_3(x) = K_2(x)\Delta p_2(x). \qquad \text{(A9)}$$

In the box approximation, the bracket equals -1 in the range (x_P, x_{P0}), assuming that $x_P < x_{P0}$. This is true for an upward Pi jump, which lowers the fraction of poststroke states (Eq. 9). Hence

$$C_{\pm}(x) = \frac{\pm\lambda_{\mp}(x)}{\lambda_+(x) - \lambda_-(x)} P(x) \qquad \text{(A10)}$$

within this range, and zero outside it. The box approximation is valid for large Pi jumps, where the ratio of initial and final concentrations is much greater than unity. Analogous statements apply for a downward jump.

Tension changes were again calculated from Eq. 6, except that the variable of integration was changed from x to $y = K_2(x)$.

Version B

Proceeding in the same way,

$$C_{\pm}(x) = \pm\frac{\dfrac{K_1}{1+K_1} k_2(x) + k_{-2}^{\text{eff}} - \lambda_{\mp}(x)}{\lambda_+(x) - \lambda_-(x)} P(x) \qquad \text{(A11)}$$

for all x in (x_P, x_{P0}) as determined by the modified form of Eq. 9.

We are grateful to K. Burton, M. A. Geeves, K. W. Ranatunga, and R. M. Simmons for discussions that prompted the development of models. We thank R. M. Simmons, J. Dantzig, and the *Journal of Physiology* for permission to reproduce published data in Fig. 2 *B* and Fig. 6.

D.A.S. acknowledges financial support from the Wellcome Trust in the initial stages of this project. D.A.S. is currently supported by National Institutes of Health grant No. R01 AR048776-01A1 and J.S. by the Medical Research Council (United Kingdom).

REFERENCES

Brenner, B. 1991. Dynamic dissociation and reassociation of actomyosin cross-bridges during force generation: a newly observed facet of cross-bridge action in muscle. *Proc. Natl. Acad. Sci. USA.* 88:10490–10494.

Chen, Y.-D., and B. Brenner. 1993. On the regeneration of the actin-myosin power stroke in contracting muscle. *Proc. Natl. Acad. Sci. USA.* 90: 5148–5152.

Conibear, P. B., C. R. Bagshaw, P. G. Fajer, M. Kovacs, and A. Malnasi-Csizmadia. 2003. Myosin cleft movement and its coupling to actomyosin dissociation. *Nat. Struct. Biol.* 10:831–835.

Cook, C. S., M. Ashley-Ross, D. Syme, Y. E. Goldman, and L. C. Rome. 1997. Trading force for speed: cross-bridge kinetics in superfast fibers. *Biophys. J.* 72:A128. (Abstr.)

Cooke, R. 1997. The mechanism of muscle contraction. *CRC Crit. Rev. Biochem.* 21:53–118.

Cooke, R., and E. W. Pate. 1995. The effects of ADP and phosphate on the contraction of muscle fibres. *Biophys. J.* 48:789–798.

Coupland, M. E., E. Puchert, and K. W. Ranatunga. 2001. Temperature dependence of active tension in mammalian (rabbit psoas) fibres: effect of inorganic phosphate. *J. Physiol.* 536:879–891.

Dantzig, J. A., Y. E. Goldman, N. C. Millar, J. Lacktis, and E. Homsher. 1992. Reversal of the cross-bridge force-generating transition by photogeneration of phosphate in rabbit psoas muscle fibres. *J. Physiol.* 451:247–278.

Davis, J. S., and M. E. Rodgers. 1995. Indirect coupling of phosphate release to de novo tension generation during muscle contraction. *Proc. Natl. Acad. Sci. USA.* 92:10482–10486.

Dobbie, I., M. Linari, G. Piazzesi, M. Reconditi, N. Koubassova, M. A. Freenczi, V. Lombardi, and M. Irving. 1998. Elastic bending and active tilting of myosin heads during muscle contraction. *Nature.* 396:383–387.

Dominguez, R., Y. Freyzon, K. M. Trybus, and C. Cohen. 1998. Crystal structure of a vertebrate smooth muscle myosin motor domain and its complex with the essential light chain: visualization of the pre-power stroke state. *Cell.* 94:559–571.

Duke, T. A. J. 1999. Molecular model of muscle contraction. *Proc. Natl. Acad. Sci. USA.* 96:2770–2775.

Eisenberg, E., T. L. Hill, and Y.-D. Chen. 1980. Cross-bridge model of muscle contraction. *Biophys. J.* 29:195–227.

Fenn, W. O. 1924. The relation between the work performed and the energy liberated in muscular contraction. *J. Physiol. (Lond.).* 58:373–395.

Fisher, A. J., C. A. Smith, J. B. Thoden, R. Smith, K. Sutoh, H. M. Holden, and I. Rayment. 1995. X-ray structures of the myosin motor domain of Dictyostelium discoideum complexed with MgADP-BeF_x and MgADP. AlF_4. *Biochemistry.* 34:8960–8972.

Ford, L. E., A. F. Huxley, and R. M. Simmons. 1977. Tension responses to sudden length change in stimulated frog muscle fibres near slack length. *J. Physiol. (Lond.).* 269:441–515.

Geeves, M. A. 1992. The actomyosin ATPase: a two-state system. *Phil. Trans. Roy. Soc.* B336:63–71.

Geeves, M. A., and K. C. Holmes. 1999. Structural basis of muscle contraction. *Annu. Rev. Biochem.* 68:687–728.

Getz, E. B., R. Cooke, and S. L. Lehman. 1998. Phase transition in force during ramp stretches of skeletal muscle. *Biophys. J.* 75:2971–2983.

Gutfreund, H., and K. W. Ranatunga. 1999. Simulation of molecular steps in muscle force generation. *Proc. Roy. Soc. B.* 266:1471–1473.

He, Z.-H., R. K. Chillingworth, M. Brune, J. E. T. Corrie, D. R. Trentham, M. R. Webb, and M. A. Ferenczi. 1997. ATPase kinetics on activation of rabbit and frog permeabilised isometric muscle fibres: a real-time phosphate assay. *J. Physiol.* 501:125–148.

Hibberd, M. G., and D. R. Trentham. 1986. Relationships between chemical and mechanical events during muscle contraction. *Annu. Rev. Biophys. Biophys. Chem.* 15:119–161.

Hilber, K., Y.-B. Sun, and M. Irving. 2001. Effects of sarcomere length and temperature on the rate of ATP utilisation by rabbit psoas muscle fibers. *J. Physiol.* 531:771–780.

Holmes, K. C. 1997. The swinging lever-arm hypothesis of muscle contraction. *Curr. Biol.* 7:R112–R118.

Holmes, K. C., I. Angert, F. J. Kull, W. Jahn, and R. R. Schroder. 2003. Electron cryo-microscopy shows how strong binding of myosin to actin releases nucleotide. *Nature.* 425:423–427.

Houdusse, A., and H. L. Sweeney. 2001. Myosin motors: missing structures and hidden springs. *Curr. Opin. Cell Biol.* 11:192–194.

Huxley, A. F. 1957. Muscle structure and theories of contraction. *Prog. Biophys. Biophys. Chem.* 7:255–318.

Huxley, A. F., and R. M. Simmons. 1971. Proposed mechanism of force generation in striated muscle. *Nature*. 233:533–538.

Huxley, H. E., A. Stewart, H. Sosa, and T. Irving. 1994. X-ray diffraction measurements of the extensibility of actin and myosin filaments in contracting muscle. *Biophys. J*. 67:2411–2421.

Huxley, A. F., and S. Tideswell. 1996. Filament compliance and tension transients in muscle. *J. Muscle Res. Cell Motil*. 17:507–511.

Kawai, M. 1986. The role of ortho-phosphate in crossbridge kinetics in chemically skinned rabbit psoas fibres as detected with sinusoidal and step length alterations. *J. Muscle Res. Cell Motil*. 7:421–434.

Linari, M., I. Dobbie, M. Reconditi, N. Koubassova, M. Irving, G. Piazzesi, and V. Lombardi. 1998. The stiffness of skeletal muscle in isometric contraction and rigor: the fraction of myosin heads bound to actin. *Biophys. J*. 74:2459–2473.

Lionne, C., F. Travers, and T. Barman. 2002. Evidence that phosphate release is the rate-limiting step on the overall ATPase of psoas myofibrils prevented from shortening by chemical cross-linking. *Biochemistry*. 41:13297–13308.

Lombardi, V., and G. Piazzesi. 1990. The contractile response during steady lengthening of stimulated frog muscle fibres. *J. Physiol*. 431: 141–171.

Lombardi, V., G. Piazzesi, and M. Linari. 1992. Rapid regeneration of the actin-myosin power stroke in contracting muscle. *Nature*. 355:638–641.

Lymn, R. W., and E. W. Taylor. 1971. Mechanism of adenosine triphosphate hydrolysis by actomyosin. *Biochemistry*. 10:4617–4624.

Millar, N. C., and E. Homsher. 1990. The effect of phosphate and calcium on force generation in glycerinated rabbit skeletal muscle fibers. A steady-state and transient kinetic study. *J. Biol. Chem*. 265: 20234–20240.

Millar, N. C., and E. Homsher. 1992. Kinetics of force generation and phosphate release in skinned rabbit soleus muscle fibers. *Am. J. Physiol*. 262:C1239–C1245.

Nishizaka, T., R. Seo, H. Tadakuma, K. Kinosita Jr., and S. Ishiwata. 2000. Characterization of single actomyosin rigor bonds: load dependence of lifetime and mechanical properties. *Biophys. J*. 79:962–974.

Pate, E., and R. Cooke. 1989. A model of crossbridge action: the effects of ATP, ADP and Pi. *J. Muscle Res. Cell Motil*. 10:181–196.

Piazzesi, G., M. Linari, M. Reconditi, F. Vanzi, and V. Lombardi. 1997. Cross-bridge detachment and attachment following a step stretch imposed on active single frog muscle fibres. *J. Physiol*. 498:3–15.

Press, W. H., B. P. Flannery, S. A. Teukolsky, and W. T. Vetterling. 1992. Numerical Recipes, 2nd ed. Cambridge University Press, UK.

Ranatunga, K. W., M. E. Coupland, and G. Mutungi. 2002. An asymmetry in the phosphate dependence of tension transients induced by length perturbations in mammalian (rabbit psoas) muscle fibres. *J. Physiol*. 542:899–910.

Rayment, I., H. M. Holden, M. Whittaker, C. B. Yohn, M. Lorenz, K. C. Holmes, and R. A. Milligan. 1993. Structure of the actin-myosin complex and its implications for muscle contraction. *Science*. 261:58–65.

Reubold, T. F., S. Eschenburg, A. Becker, F. J. Kull, and D. J. Manstein. 2003. A structural model for actin-induced nucleotide release in myosin. *Nat. Struct. Biol*. 10:826–830.

Siemankowski, R. F., M. O. Wiseman, and H. D. White. 1985. ADP dissociation from actomyosin subfragment 1 is sufficiently slow to limit the unloaded shortening velocity in vertebrate muscle. *Proc. Natl. Acad. Sci. USA*. 82:658–662.

Sleep, J. A., and R. L. Hutton. 1980. Exchange between inorganic phosphates and adenosine 5′-triphosphate in the medium by actomyosin subfragment 1. *Biochemistry*. 19:1276–1283.

Smith, D. A. 1998. Strain-dependent ratchet model for [phosphate]- and [ATP]-dependent muscle contraction. *J. Muscle Res. Cell Motil*. 19: 189–212.

Smith, D. A., and M. A. Geeves. 1995. Strain-dependent cross-bridge cycle for muscle. *Biophys. J*. 69:524–537.

Tesi, C., F. Colomo, S. Nencini, N. Pirrodi, and C. Poggesi. 2000. The effect of inorganic phosphate on force generation in single myofibrils from rabbit skeletal muscle. *Biophys. J*. 78:3081–3092.

Wakabayashi, K., Y. Sugimoto, H. Tanaka, Y. Takezawa, and Y. Amemiya. 1994. X-ray diffraction evidence for the extensibility of actin and myosin filaments during muscle contraction. *Biophys. J*. 67: 2422–2435.

White, H. D., B. Belknap, and M. R. Webb. 1997. Kinetics of nucleoside triphosphate cleavage and phosphate release steps by associated rabbit skeletal actomyosin, measured using a novel fluorescent probe for phosphate. *Biochemistry*. 36:11828–11836.

Wood, J. E., and R. W. Mann. 1981. A sliding-filament cross-bridge ensemble model of muscle contraction for mechanical transients. *Math. Biosci*. 57:211–263.

Yount, R. G., D. Lawson, and I. Rayment. 1995. Is myosin a ''back door'' enzyme? *Biophys. J*. 68:47S–49S.